Appl. Phys. A 71, 503–510 (2000) / Digital Object Identifier (DOI) 10.1007/s003390000706

Applied Physics A
Materials
Science & Processing

Self-energy and inelastic lifetimes of surface-state electrons and holes in metals

P.M. Echenique[1,2,*], J. Osma[1], V.M. Silkin[2], E.V. Chulkov[1,2], J.M. Pitarke[2,3]

[1] Materialen Fisika Saila, Kimika Fakultatea, Euskal Herriko Unibertsitatea, 1072 Posta kutxatila, 20018 Donostia, Basque Country, Spain
[2] Donostia International Physics Center (DIPC) and Centro Mixto CSIC-UPV/EHU, Donostia, Basque Country, Spain
[3] Materia Kondentsatuaren Fisika Saila, Zientzi Fakultatea, Euskal Herriko Unibertsitatea, 644 Posta kutxatila, 48080 Bilbao, Basque Country, Spain

Received: 13 April 2000/Accepted: 2 September 2000/Published online: 12 October 2000 –

Abstract. A metal surface generates electron states that do not exist in a bulk metal. These so-called surface states can be classified into two categories, crystal-induced (intrinsic) states and image-potential-induced (image) states. Here we present a survey of current investigations on the origin of the decay of these surface states. Inelastic lifetimes are obtained from the knowledge of the quasiparticle self-energy, which we compute, within the GW approximation of many-body theory, by going beyond a free-electron description of the surface. Surface-state lifetimes in noble metal surfaces are presented. Our results show that actual lifetimes are highly sensitive to the details of the surface response and to the presence of the intrinsic surface state itself.

PACS: 73.20.At; 72.15.Lh; 73.20.Dx

A quantity of basic interest in the description of many-electron Fermi liquids is the quasiparticle lifetime [1]. It is well known that inelastic lifetimes govern the dynamics of charge transfer and electronic excitations in the bulk and at the surface of solid materials, and they play a key role in a variety of physical and chemical phenomena [2, 3]. Here we focus on the theoretical description of the lifetime of elementary excitations that are generated by the presence of a metal surface. These are intrinsic surface states of the s-p_z symmetry and image-potential-induced surface states [4].

Intrinsic surface states are localized near the crystal surface, the surface-state wave function being monotonically damped in the direction of the vacuum. Image states are localized in the vacuum region of the surface, the corresponding wave functions being nearly decoupled from bulk states. The dispersion of both intrinsic and image surface states with the wave vector $\boldsymbol{k}_\parallel$ parallel to the surface is found to be parabolic, i.e., $E = \varepsilon + \hbar^2\boldsymbol{k}_\parallel^2/(2m)$, where ε describes motion normal to the surface and m is the effective mass. While the energy ε of intrinsic surface states is found to be near the Fermi level $E_{\rm F}$, image states are just below the vacuum level and form a Rydberg-like series with binding energies $\varepsilon_n = 0.85/(n+a)^2$eV $(n \geq 1)$, a being the so-called quantum defect [4, 5]. A comparison of crystal-induced and image-potential surface states is given in Fig. 1.

Unoccupied image-potential states were detected on the surfaces of Cu, Ag, and Ni by using inverse [6–8] and two-photon [9] photoemission techniques. In combination with the use of ultrafast lasers, accurate measurements of the linewidth of image states on metal surfaces have been carried out with the use of two-photon photoemission (2PPE) [10] and time-resolved 2PPE (TR-2PPE) spectroscopy [11–17]. Photohole lifetimes of crystal-induced surface states in a variety of metal surfaces have been investigated with high-resolution angle-resolved photoemission (ARP) spectroscopy [18–23]. Recently, the scanning tunneling microscope (STM) has been used to determine the lifetime of excited holes at the edge of the partially occupied surface state on the (111) face of noble metals [24, 25], and also to measure the lifetime of hot surface-state and surface-resonance electrons, as a function of energy [26].

In a heuristic approach, the inelastic broadening of surface states has been expected to be given by the broadening of a bulk state of the same energy times the penetration of the surface-state wave function into the bulk (for the intrinsic surface state this penetration is close to unity, but in the case of image-potential states it may be as low as ~ 0.03). Nevertheless, contributions to the surface-state decaying mechanism coming from either the evanescent tails of bulk states outside the crystal or the presence of the crystal-induced surface state itself are found to be of crucial importance [25, 27–30]. Hence, for a quantitative prediction of the lifetime of either intrinsic or image surface states, self-consistent many-body surface calculations that go beyond a free-electron description of the bounded electron gas must be carried out [27].

In this paper, we present an analysis of the role that the partially occupied Cu(111) and Ag(111) intrinsic surface states play in the relaxation of (a) holes excited in the occupied part of the surface state itself, and (b) image states. We present self-consistent calculations of the screened interaction, the self-energy, and the surface-state inelastic lifetime along the lines of [27], and account for the potential variation

*Corresponding author.
(Fax: +34-943/015-600, E-mail: wapetlap@sq.ehu.es)

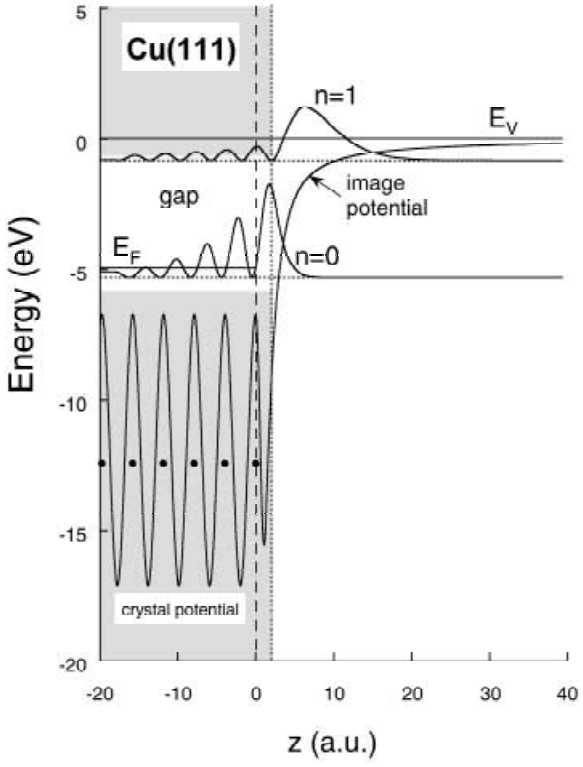

Fig. 1. One-dimensional model potential for the (111) surface of Cu. This model potential approaches the classical image potential, far outside the surface. It also reproduces the position of the upper and lower edge of the band gap at the $\overline{\Gamma}$ point ($\boldsymbol{k}_{\parallel} = 0$), which are -0.9 and 4.23 eV with respect to the Fermi level E_F. The crystal termination yields the $n = 0$ intrinsic surface state just below the Fermi level. The image potential leads to a Rydberg-like series of bound states, the so-called image states, near the vacuum level. For the $n = 0$ crystal-induced and the $n = 1$ image-potential-induced surface states, the probability-density $|\phi_n(z)|^2$ is also shown

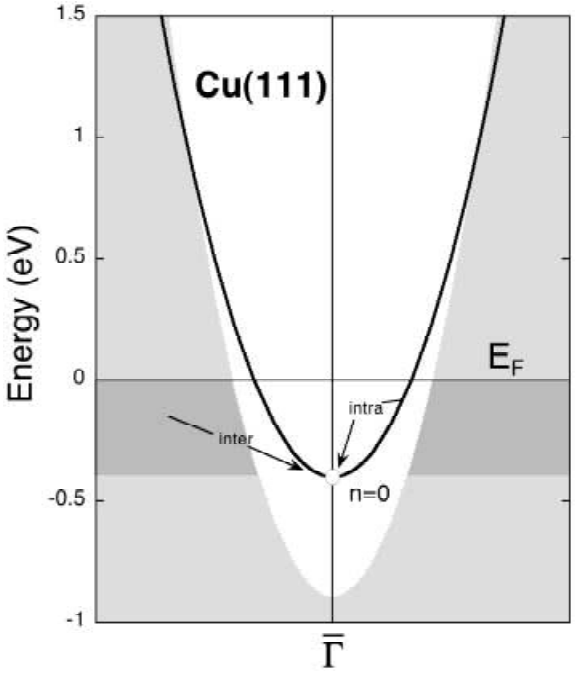

Fig. 2. Dispersion of the $n = 0$ intrinsic surface state on Cu(111) (*solid line*). *Shaded areas* represent the areas outside the band gap, where bulk states exist

parallel to the surface through the introduction of the effective mass. Since the quasiparticle decay of an intrinsic surface state may proceed (see Fig. 2) through the coupling with bulk states (3D channel) and through the coupling, within the surface state itself, with surface states of different wave vector parallel to the surface (2D channel), we also consider the decay rate of electrons or holes in three-dimensional (3D) and two-dimensional (2D) uniform systems.

1 Theory

Let us consider an inhomogeneous electron system. In the framework of many-body theory, the decay rate of either an excited electron ($E > E_{\mathrm{F}}$) or an excited hole ($E < E_{\mathrm{F}}$) in the state $\phi(\boldsymbol{r})$ with energy E is obtained as the projection of the imaginary part of the electron/hole self-energy $\Sigma(\boldsymbol{r}, \boldsymbol{r}'; E)$ over the state itself (atomic units are used in this section, i.e., $e^2 = \hbar = m_e = 1$):

$$\tau^{-1} = -2 \int \mathrm{d}\boldsymbol{r} \int \mathrm{d}\boldsymbol{r}'\, \phi^*(\boldsymbol{r})\, \mathrm{Im}\, \Sigma(\boldsymbol{r}, \boldsymbol{r}'; E)\, \phi(\boldsymbol{r}')\,. \tag{1}$$

In the GW approximation, one considers only the first-order term in a series expansion of the self-energy in terms of the screened Coulomb interaction:

$$\Sigma(\boldsymbol{r}, \boldsymbol{r}'; E) = \frac{i}{2\pi} \int dE'\, G(\boldsymbol{r}, \boldsymbol{r}'; E - E')\, W(\boldsymbol{r}, \boldsymbol{r}'; E')\,, \tag{2}$$

where $G(\boldsymbol{r}, \boldsymbol{r}'; E)$ represents the one-particle Green function and $W(\boldsymbol{r}, \boldsymbol{r}'; E)$ is the so-called screened Coulomb interaction,

$$W(\boldsymbol{r}, \boldsymbol{r}'; E) = \int d\boldsymbol{r}'' \epsilon^{-1}(\boldsymbol{r}, \boldsymbol{r}''; E)\, v(\boldsymbol{r}'' - \boldsymbol{r}')\,. \tag{3}$$

Here, $v(\boldsymbol{r} - \boldsymbol{r}')$ represents the bare Coulomb interaction, and $\epsilon^{-1}(\boldsymbol{r}, \boldsymbol{r}'; E)$ is the inverse dielectric function of the electron system.

After replacing the Green function (G) by the zero-order approximation (G^0), the imaginary part of the self-energy is obtained as

$$\mathrm{Im}\, \Sigma(\boldsymbol{r}, \boldsymbol{r}'; E) = \sum_f \phi_f^*(\boldsymbol{r}') \mathrm{Im}\, W(\boldsymbol{r}, \boldsymbol{r}'; |E - E_f|) \phi_f(\boldsymbol{r})\,, \tag{4}$$

where the sum is extended over a complete set of final states $\phi_f(\boldsymbol{r})$ with energy E_f $\left[0 \le |E - E_f| \le |E - E_{\mathrm{F}}|\right]$.

We first consider a uniform 3D or 2D degenerate electron gas, thus single-particle wave functions being simply plane waves. The decay rate of an excited electron or hole with momentum $\boldsymbol{k}$ and energy $E = \boldsymbol{k}^2/2$ is then found from (1) and (4) to be given by the following expression:

$$\tau^{-1} = 2 \int \frac{\mathrm{d}\boldsymbol{q}}{(2\pi)^3}\, v_{\boldsymbol{q}}\, \mathrm{Im}\left[-\epsilon^{-1}_{\boldsymbol{q},\omega}\right]\,, \tag{5}$$

where $v_{\boldsymbol{q}}$ and $\epsilon_{\boldsymbol{q},\omega}$ represent the Fourier transform of the bare Coulomb interaction and the dielectric function, respectively, and $\omega = \left|\boldsymbol{q}\cdot\boldsymbol{k} - q^2/2\right|$ is the energy transfer. In 3D, $v_{\boldsymbol{q}} = 4\pi/q^2$ and $\epsilon_{\boldsymbol{q},\omega}$ is, within RPA, the dielectric function

of Lindhard [31]. In 2D, $v_{\boldsymbol{q}} = 2\pi/q$ and the RPA dielectric function $\epsilon_{\boldsymbol{q},\omega}$ is that first derived by Stern [32].

For electrons/holes near the Fermi level, i.e., $|E - E_{\rm F}| \ll E_{\rm F}$, the frequency entering the so-called energy-loss function $\mathrm{Im}\left[-\epsilon^{-1}_{\boldsymbol{q},\omega}\right]$ is small ($\omega \ll E_{\rm F}$), and the momentum transfer is always smaller than $\sim 2q_{\rm F}$. Making use of the small q and ω expansion of the dielectric function, one finds the following 3D and 2D decay rates [33]:

$$\tau^{-1}_{\rm 3D} = \frac{q^2_{\rm F}/k}{32\left[1-\left(q^{\rm TF}_{\rm 3D}/2q_{\rm F}\right)^{2/3}\right]}\left[\frac{1}{\alpha}\,\tan^{-1}\frac{1}{\alpha}+\frac{1}{1+\alpha^2}\right] \times\left(\frac{E-E_{\rm F}}{E_{\rm F}}\right)^2, \tag{6}$$

where

$$\alpha = \frac{q^{\rm TF}_{\rm 3D}/2q_{\rm F}}{\sqrt{1-\left(q^{\rm TF}_{\rm 3D}/2q_{\rm F}\right)^{2/3}}}, \tag{7}$$

and [34, 35]

$$\tau^{-1}_{\rm 2D} = \frac{E_{\rm F}}{4\pi}\left[-\ln\frac{E-E_{\rm F}}{E_{\rm F}}+\frac{1}{2}+\ln\frac{2q^{\rm TF}_{\rm 2D}}{q_{\rm F}}\right]\left(\frac{E-E_{\rm F}}{E_{\rm F}}\right)^2. \tag{8}$$

Here, $q^{\rm TF}_{\rm 3D}$ and $q^{\rm TF}_{\rm 2D}$ are the Thomas-Fermi screening wave vectors in 3D and 2D, given by $\sqrt{4q_{\rm F}/\pi}$ and 2, respectively.

In the case of a bounded 3D electron gas that is translationally invariant in the plane of the surface, the decay rate of an excited electron or hole in the state $\phi(z)\mathrm{e}^{i\boldsymbol{k}_\parallel\cdot\boldsymbol{r}_\parallel}$ with energy $E = \varepsilon + \boldsymbol{k}^2_\parallel/(2m)$ is found from (1) to be given by the following expression:

$$\tau^{-1} = -2\int \mathrm{d}z \int \mathrm{d}z'\phi^*(z)\mathrm{Im}\Sigma(z,z';\boldsymbol{k}_\parallel,E)\phi(z'), \tag{9}$$

where $\Sigma(z,z';\boldsymbol{k}_\parallel,E)$ is the two-dimensional Fourier transform of the quasiparticle self-energy (see (4))

$$\mathrm{Im}\,\Sigma(z,z';\boldsymbol{k}_\parallel,E) = \sum_f \int \frac{\mathrm{d}\boldsymbol{q}_\parallel}{(2\pi)^2}\phi^*_f(z') \times \mathrm{Im}W(z,z';\boldsymbol{q}_\parallel,|E-E_f|)\,\phi_f(z), \tag{10}$$

and

$$E_f = \varepsilon_f + \frac{(\boldsymbol{k}_\parallel+\boldsymbol{q}_\parallel)^2}{2\,m_f}. \tag{11}$$

The sum in (10) is extended over a complete set of final states $\phi_f(z)$ with energy ε_f $[0 \le |E-E_f| \le |E-E_{\rm F}|]$, and $W(z,z';\boldsymbol{q}_\parallel,\omega)$ represents the two-dimensional Fourier transform of the screened interaction.

For a realistic description of the metal surface, we compute the surface-state wave function $\phi(z)$, the final states $\phi_f(z)$, and all the one-electron eigenfunctions entering the non-interacting density response function, by solving a single-particle time-independent Schrödinger equation with a realistic one-dimensional model potential [36]. This model potential, which approaches far outside the surface the classical image potential, reproduces the width and position of the energy gap at the $\overline{\Gamma}$ point ($\boldsymbol{k}_\parallel = 0$) as well as the binding energies of both the $n = 0$ (intrinsic) and $n = 1$ (first-image) surface states at $\overline{\Gamma}$. We also account for the change of the z-dependent surface-state wave functions along the dispersion curve, by recalculating them with $\boldsymbol{k}_\parallel \neq 0$ as was done at the $\overline{\Gamma}$ point. Departure of the motion along the surface from free-electron behavior is accounted through the introduction of the effective mass m and m_f of the quasiparticle initial and final state, respectively. The screened interaction is computed within the random-phase approximation (RPA) [37], from the knowledge of the non-interacting density response function [38]. Finally, the GW approximation is used to compute the electron or hole self-energy and the decay rate.

2 Results and discussion

On the (111) surfaces of Cu and Ag, the $n = 0$ surface state at the center of the surface Brillouin zone ($\boldsymbol{k}_\parallel = 0$) lies just below the Fermi level, with $\varepsilon_0 - E_{\rm F} = -445$ and -67 meV, respectively. In the case of Cu(111) (see Fig. 2), for energies $E_0 - E_{\rm F} > 1$ eV $[E_0 = \varepsilon_0 + k^2_\parallel/(2m)]$ this partially occupied surface-state band lies outside the projected band gap, thereby becoming a surface resonance. Binding energies of the $n = 1$ image state on Cu(111) and Ag(111) (measured with respect to the vacuum level) are 0.83 and 0.77 eV, respectively. Effective masses of the $n = 1$ image state on the (111) surfaces of Cu and Ag have been reported to be 1.0 and 1.3, respectively [10], while the effective masses of the $n = 0$ state on these surfaces are 0.42 and 0.44 [39, 40]. For bulk states entering (10), we have chosen to increase the effective mass from our computed value of $m_f = 0.31$ and 0.25 at the bottom of the gap in Cu(111) and Ag(111), to $m_f = 1$ at the bottom of the valence band.

Probability densities, $|\phi_n(z)|^2$, for the $n = 0$ and $n = 1$ surface states on Cu(111), as obtained by solving the Schrödinger equation with the one-dimensional potential of [36], are exhibited in Fig. 1. The corresponding probability densities for the $n = 0$ and $n = 1$ surface states on Ag(111) present a similar behavior. Both $n = 0$ and $n = 1$ surface-state wave functions are localized in the direction perpendicular to the crystal surface; however, while the $n = 0$ surface-state wave function is located at the crystal edge, which we choose to be located half a lattice spacing beyond the last atomic layer, the $n = 1$ image-state wave function is located well-outside the crystal. The Cu(111) and Ag(111) $n = 1$ probability-density maxima occur at $z_1 = 2.3$ Å and $z_1 = 2.5$ Å (measured with respect to the crystal edge), respectively.

Figure 3 shows self-consistent RPA calculations of the imaginary part of the screened interaction $W(z,z';\boldsymbol{q}_\parallel,\omega)$ in the vicinity of the (111) surface of Cu. This quantity is represented as a function of z for fixed values of $q_\parallel[q_\parallel = 0.5\,a_0^{-1}]$, $\omega[\omega = 0.5$ eV], and z'. In the bottom panel, z' is fixed a few atomic layers within the bulk. When z' is fixed at the crystal edge (middle panel), which nearly coincides with the maximum of the $n = 0$ probability density, we find that $\mathrm{Im}\left[-W(z,z;\boldsymbol{q}_\parallel,\omega)\right]$ is considerably larger than within the bulk. The top panel corresponds to z' being fixed near the maximum of the Cu(111) and Ag(111) $n = 1$ probability densities. One clearly sees that the maximum magnitude of $\mathrm{Im}\left[-W(z,z;\boldsymbol{q}_\parallel,\omega)\right]$ occurs at $z \sim 0$ rather than for $z = z'$, showing a highly nonlocal behav-

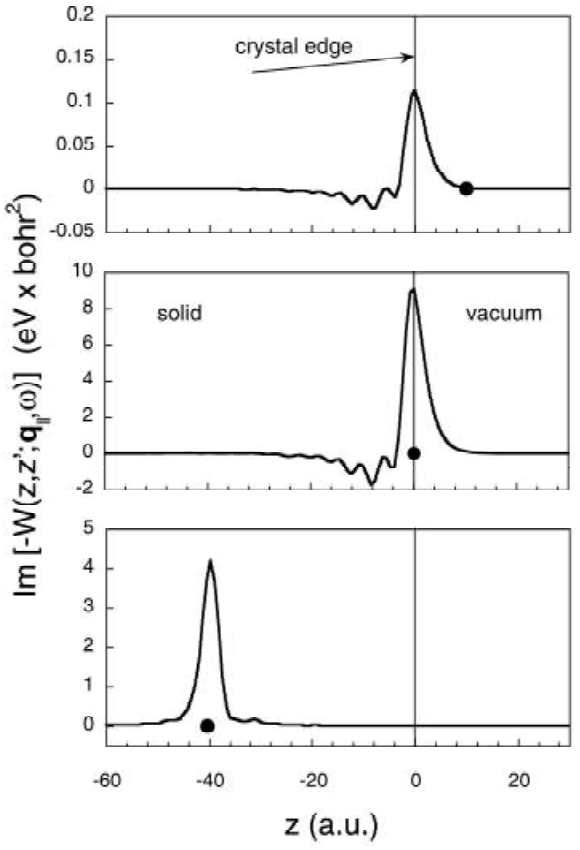

Fig. 3. Imaginary part of the RPA screened interaction $\mathrm{Im}\left[-W(z,z';\boldsymbol{q}_\parallel,\omega)\right]$, versus z, in the vicinity of the (111) surface of Cu. $q_\parallel$ and ω are taken to be $q_\parallel = 0.5\,a_0^{-1}$ and $\omega = 0.5$ eV. z' is fixed at -41 (*bottom panel*), 0 (*middle panel*), and $10\,a_0$ (*top panel*)

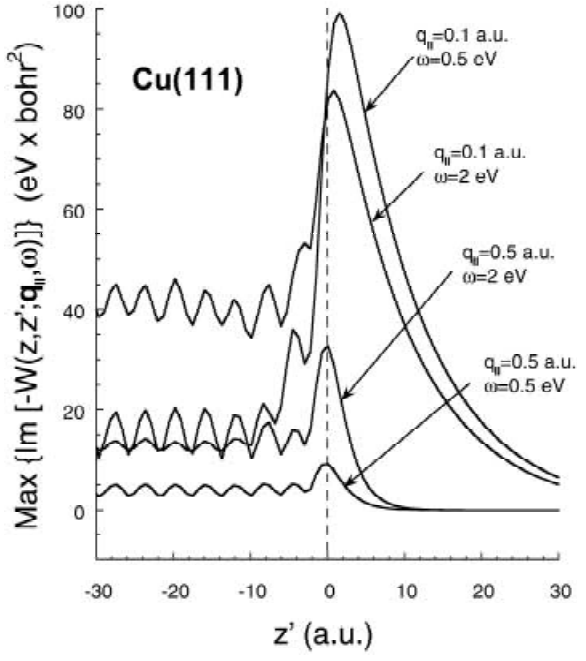

Fig. 4. Maximum of the imaginary part of the RPA screened interaction $\mathrm{Im}\left[-W(z,z';\boldsymbol{q}_\parallel,\omega)\right]$, versus z', in the vicinity of the (111) surface of Cu, for various values of $q_\parallel$: 0.1 and $0.5\,a_0^{-1}$, and for various values of ω: 0.5 and 2 eV

ior of this quantity. We also note that far from the crystal, into the vacuum, the imaginary part of the screened interaction is, at the same energy, well below that in the bulk and near the surface.

That the maximum magnitude of $\mathrm{Im}\left[-W(z,z';\boldsymbol{q}_\parallel,\omega)\right]$ is enhanced near the surface and quickly decreases as z' is located far from the crystal into the vacuum is clearly shown in Fig. 4. In this figure, the magnitude of the maximum of $\mathrm{Im}\left[-W(z,z';\boldsymbol{q}_\parallel,\omega)\right]$ is plotted, as a function of z' and for various values of $q_\parallel$ and ω. This figure shows that electron–hole pair creation takes place mainly in the vicinity of the surface. For $q_\parallel = 0.5\,a_0^{-1}$ one sees that $\mathrm{Im}\left[-W(z,z';\boldsymbol{q}_\parallel,\omega)\right]$ increases with ω for all values of z', showing that for this value of $q_\parallel$ major contributions to the decay rate come from the largest possible energy transfers. This figure also shows that major contributions to the decay rate come from small values of the parallel component of the momentum transfer. Nevertheless, for these small values of $q_\parallel$ the imaginary part of the screened interaction increases with the energy transfer only within the bulk, major contributions to the decay rate coming at the surface and within the vacuum from the smallest energy transfers.

Figures 5 and 6 show full self-consistent RPA calculations of the imaginary part of the $n = 0$ surface-state hole and the $n = 1$ image-electron self-energy $\mathrm{Im}\left[-\Sigma(z,z';\boldsymbol{k}_\parallel = 0, E_n)\right]$ in the vicinity of the (111) surface of Cu, as obtained from (10). The imaginary part of the self-energy is represented in these figures as a function of z and for a fixed value of z'. In the bottom panel, z' is fixed a few atomic layers within the bulk, showing that $\mathrm{Im}(-\Sigma)$ has a maximum at $z = z'$, as in the case of a homogeneous electron gas. When z' is fixed at the crystal edge ($z' \sim 0$), as shown in the middle panel of Figs. 5 and 6, we find that $\mathrm{Im}(-\Sigma)$ is still maximum at $z = z'$, but the magnitude of this maximum is now enhanced. The top panel of Figs. 5 and 6 corresponds to z' being fixed far from the surface into the vacuum. In this case, the maximum magnitude of $\mathrm{Im}(-\Sigma)$ occurs at $z \sim 0$ rather than for $z = z'$, as occurs in the case of the imaginary part of the screened interaction. As the phase-space available for real transitions from the $n = 1$ image state is larger than from the excited hole at the edge of the $n = 0$ surface state $[\varepsilon_1 - E_\mathrm{F} > E_\mathrm{F} - \varepsilon_0]$, the imaginary part of the $n = 1$ image-state self-energy is larger than in the case of the $n = 0$ surface-state hole. Dotted lines in Fig. 5 represent the contribution to the imaginary part of the $n = 0$ surface-state hole self-energy from transitions to the $n = 0$ surface state itself, the so-called intraband transitions. One sees that within the vacuum side of the surface, intraband transitions dominate, while within the bulk they represent a minor contribution.

In Figs. 7 and 8, separate contributions to the magnitude of the maximum of $\mathrm{Im}(-\Sigma)$ for the $n = 0$ and $n = 1$ surface states are plotted, according to whether only transitions to the $n = 0$ intrinsic surface state (dotted line) or all available transitions (solid line) are included. The imaginary part of the $n = 1$ image-state self-energy maximum is clearly larger than in the case of the $n = 0$ surface-state hole, simply due to the larger departure of the image-state energy from the Fermi level, as noted above.

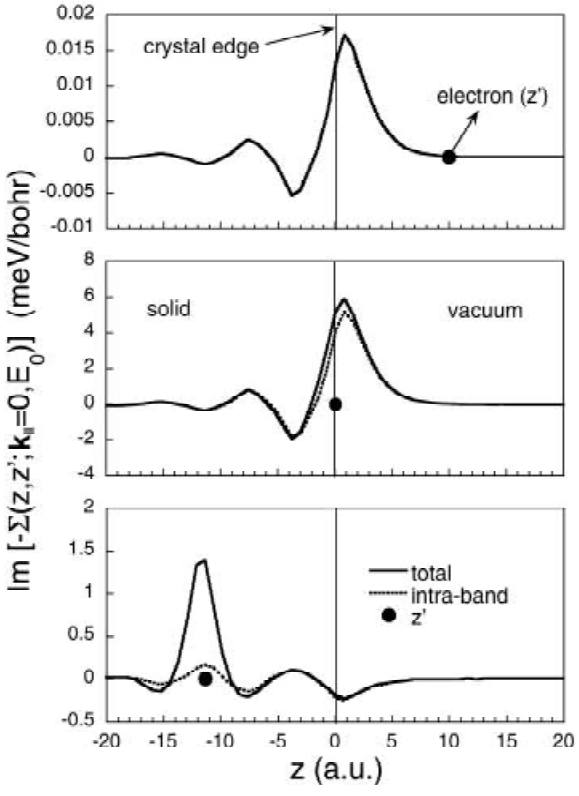

Fig. 5. Imaginary part of the self-energy of the $n = 0$ surface-state hole, $\mathrm{Im}\left[-\Sigma(z, z'; \boldsymbol{k}_{\parallel} = 0, E_0)\right]$, versus z, in the vicinity of the (111) surface of Cu, as obtained from (10) with use of the full RPA screened interaction. $\acute{z}$ is fixed at -11.3 (*bottom panel*), 0 (*middle panel*), and $10\,a_0$ (*top panel*). *Dotted lines* represent the contribution from transitions to the $n = 0$ surface state itself

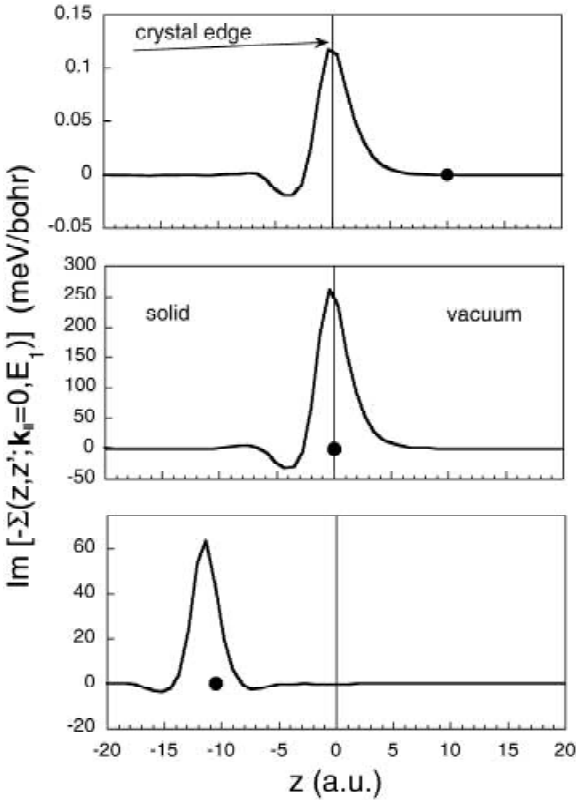

Fig. 6. As in Fig. 5, for the imaginary part of the self-energy of the $n = 1$ image-state electron

2.1 Intrinsic surface-state holes

Now we focus on the evaluation of the decay rate of intrinsic ($n = 0$) surface-state holes on the (111) surfaces of Cu and Ag. Coupling of the $n = 0$ surface state with the crystal occurs either with bulk states (interband transition) or within the $n = 0$ surface-state band itself (intraband transition). These separate contributions to the decay rate of excited holes at the $n = 0$ surface-state band edge ($\boldsymbol{k}_{\parallel} = 0$) in Cu(111) and Ag(111), as obtained from (9), are exhibited in Table 1. One sees that intraband transitions within the $n = 0$ surface state contribute $\sim 80\%$–90% to the total decay rate, showing that these transitions are more efficient in filling the hole relative to interband transitions. As the wave vector parallel to the surface increases and, therefore, the energy of the surface-state hole approaches the Fermi energy, the hole penetrates more into the bulk and the relative contribution from intraband transitions is expected to decrease [41].

Decay rates for a hole in a uniform 3D electron gas at the energy of the $n = 0$ surface-state band edge in Cu(111) and Ag(111), as obtained from (5) with use of the full RPA dielectric function, are also shown in Table 1 [42], showing that they are close to the actual interband contribution. Nevertheless, this is the result of two competing effects. As the surface-state wave function is localized at the surface, the actual screened interaction (see Figs. 3 and 4) yields larger decay rates than those predicted by (5), and this enhancement of the decay rate is partially compensated by the restriction not included in (5) that only final states with energy E_f lying below the projected band gap are allowed. In the case of Cu(111) this compensation is nearly complete; however, this is not necessarily the case for other materials, depending on the relative amount of final states that are not allowed for small values of the component of the momentum transfer that is parallel to the surface. For Ag(111), the relative number of forbidden final states is small, and the actual interband contribution to the linewidth is about 1.7 times larger than predicted within a uniform 3D electron-gas model.

The partially occupied $n = 0$ surface-state band on the (111) surfaces of Cu and Ag forms a uniform 2D electron gas, with the 2D Fermi energy being given by the band edge of the surface state, i.e., $E_{\mathrm{F}}^{\mathrm{2D}} = -\varepsilon_0$, and the electron mass being equal to the surface-state effective mass. We have calculated from (5) the decay rate of an excited hole at the bottom of the $n = 0$ surface-state band in Cu(111) and Ag(111) [$E - E_{\mathrm{F}}^{\mathrm{3D}} = -E_{\mathrm{F}}^{\mathrm{2D}} = -445$ meV and -67 meV, respectively],

Table 1. GW-RPA decay rates, in linewidth units (meV), of the $n = 0$ intrinsic surface state at the $\overline{\Gamma}$ point ($\boldsymbol{k}_{\parallel} = 0$) on the (111) surfaces of Cu and Ag, as obtained from (9). Contributions to the linewidth from decay into the $n = 0$ surface state itself are displayed in parentheses. GW-RPA decay rates for a hole in a uniform 3D and 2D electron gas at the energy of the $n = 0$ surface-state band edge are also displayed. The experimentally determined decay rates are taken from [24]

Surface	Energy (meV)	Linewidth	2D	3D	Experiment
Cu(111)	-445	25(19)	127	5.9	24
Ag(111)	-67	3(2.7)	20	0.18	6

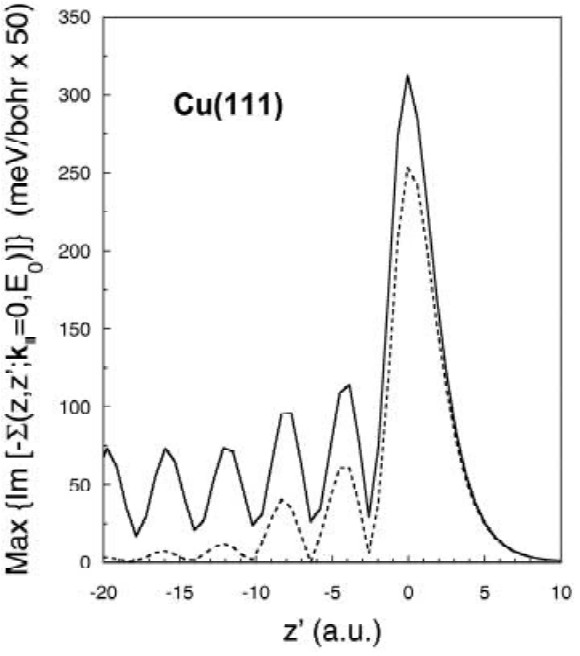

Fig. 7. Maximum of the imaginary part of the $n = 0$ surface-state hole self-energy, $\mathrm{Im}\left[-\Sigma(z, z'; \boldsymbol{k}_\parallel = 0, E_0)\right]$, versus z', in the vicinity of the (111) surface of Cu, as obtained from (10) with the use of the full RPA screened interaction. *Dotted lines* represent the contribution from transitions to the $n = 0$ surface state itself

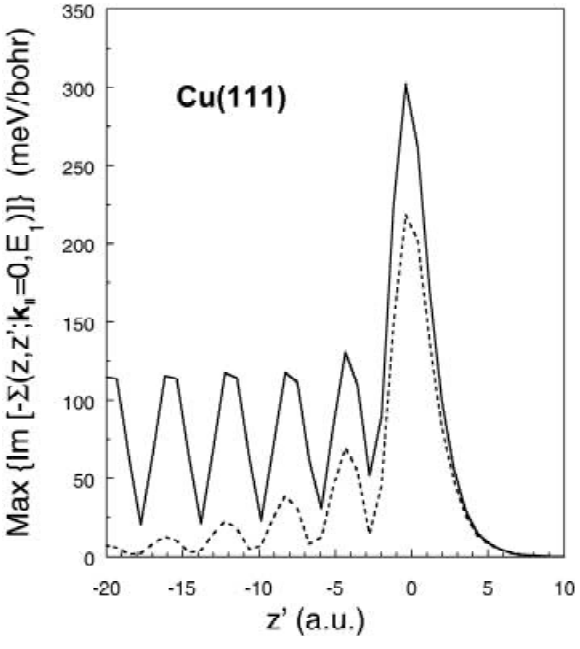

Fig. 8. As in Fig. 7, for the imaginary part of the $n = 1$ image-state electron self-energy. *Dotted lines* represent the contribution from transitions to the $n = 0$ surface state

and have obtained, with use of the full 2D RPA dielectric function, the results shown in Table 1 [43]. We note that the result of these calculations is larger than the actual intraband contribution by a factor of ~ 7. This large discrepancy is due to the fact that electron–electron interactions within the actual $n = 0$ surface-state 2D band are strongly screened by the underlying 3D bulk electron system, thus yielding smaller decay rates than within a pure 2D electron gas. Although the 2D Fermi energy in Cu(111) is considerably larger than that in Ag(111), 3D screening effects in both materials are found to be comparable [44].

Also shown in Table 1 are recent low-temperature STM measurements [24, 25] of the excited hole at the edge of the partially occupied $n = 0$ surface state on the (111) surfaces of Cu and Ag. At this point, we note that one must be cautious in the comparison of STM measurements with our calculations. On the one hand, electron-phonon scattering is expected to yield contributions to the experimentally measured linewidths of 8.0 and 5.2 meV for Cu and Ag, respectively [19], which would result in measured inelastic linewidths of 16 and 0.8 meV for these materials. [For Cu(111), an extrapolation of the ARP linewidth to zero defect density yields a linewidth of 21 meV [20].] On the other hand, our model potential correctly reproduces the behavior of the *s*-*p* valence states, but it does not include screening from *d*-electrons. The effect of virtual interband transitions giving rise to additional screening by *d*-electrons is to decrease the linewidth, for energies very near the Fermi level [45], as discussed in [25]. We also note that while 3D bulk calculations qualitatively account for the interband contribution to the hole-lifetime, our results indicate that intraband transitions represent the main contribution to the measured lifetime.

2.2 Image-state electrons

Our self-consistent calculations of the linewidth of the $n = 1$ image state on the (111) surfaces of Cu and Ag, as obtained from (9) at the $\overline{\Gamma}$ point ($\boldsymbol{k}_\parallel = 0$) and with use of the full RPA screened interaction, are presented in Table 2, together with recent experimental measurements [13–15]. Coupling of the $n = 1$ image-state electron with the solid occurs either with bulk states or with the unoccupied part of the $n = 0$ surface-state band. Hence, separate contributions to the $n = 1$ image-state linewidth are given in Table 2, according to whether only transitions to the $n = 0$ intrinsic surface state or all available transitions are included. As in the case of the $n = 0$ intrinsic surface-state hole, there is a large contribution to τ^{-1} from the decay into the $n = 0$ surface-state band, lying within the projected band gap, which in both Cu(111) and Ag(111) approximately represents 35%–40% of the total decay rate.

Decay rates for an electron in a uniform 3D electron gas at the energy of the $n = 1$ image state on Cu(111) and Ag(111), as obtained from (5) with use of the full RPA dielectric function, are also shown in Table 2 [42]. These decay rates times

Table 2. GW-RPA decay rates, in linewidth units (meV), of the $n = 1$ image-state electron at the $\overline{\Gamma}$ point ($\boldsymbol{k}_\parallel = 0$) on the (111) surfaces of Cu and Ag and the (0001) surface of Ru. Contributions to the linewidth from decay into the unoccupied part of the $n = 0$ surface state are displayed in parentheses. GW-RPA decay rates for an electron in a uniform 3D electron gas at the energy of the $n = 1$ image-state electron at $\overline{\Gamma}$ are also displayed. The experimentally determined decay rates are taken from [13], [14], and [15], for Cu(111), Ag(111), and Ru(0001), respectively

Surface	Energy (eV)	Linewidth	3D	Experiment
Cu(111)	-0.83	29(12)	301	30
Ag(111)	-0.77	37(13)	330	22
Ru(0001)	-0.64	14		11

the penetration (the penetration amounts to 0.22 and 0.25 in the case of Cu(111) and Ag(111), respectively) are found to be too large and cannot explain the actual image-state linewidth, not even that part of the linewidth coming from transitions to bulk states. This is due to the large restriction, not included in (5), that only final states with energy E_f lying below the projected band gap are allowed. On the (111) surfaces of Cu and Ag, the binding energy of the $n = 1$ image state is close to the top of the *sp*-band gap, which extends below the Fermi level, and the available phase space becomes, therefore, highly restricted.

Although the $n = 1$ image state on Ag(111) is closer to the Fermi level than in the case of Cu(111), a weaker screening in Ag (the electron-density parameter in Ag is larger than in Cu) yields an image-state linewidth that is larger on this surface. Nevertheless, this is not in agreement with the experimental measurements, which show that the $n = 1$ image-state lifetime on the (111) surface of Ag is smaller than on the (111) surface of Cu. While the experimental measurement for Cu(111) is in excellent agreement with our full GW-RPA prediction, our calculations yield a linewidth for Ag(111) that is too high. This discrepancy may have originated in the presence of the well-known low-energy plasmon excitation in this material, not present in our one-dimensional model.

Finally, we consider the $n = 1$ image state on the (0001) surface of ruthenium. This surface presents a projected band gap at $\boldsymbol{k}_{\parallel} = 0$ of 7.3 eV (the upper and lower edge are located at 1.4 and 8.7 eV with respect to the Fermi level), and the $n = 1$ image state is found to be located close to the band-gap center, at 0.57 eV below the vacuum level. Hence, the $n = 1$ image-state wave-function overlap with the bulk ($p = 0.03$) is much smaller than in the case of the (111) surfaces of Cu and Ag. Nevertheless, the available phase space on Ru(0001) is not as restricted as in the case of Cu(111) and Ag(111), and the $n = 1$ image-state linewidth on Ru(0001) is found to be comparable to that found for Cu(111) and Ag(111). Our calculated linewidth of the $n = 1$ image state on this surface is found to be in fair agreement with the recent measurements reported in [15].

3 Summary and conclusions

We have reported a survey of current investigations on the origin and measure of the decay of either crystal or image-potential-induced surface states. We have presented full GW-RPA many-body self-consistent calculations of the screened interaction, the self-energy, and the surface-state inelastic lifetimes. We have reached the important conclusion that contributions to the surface-state decaying mechanism coming from either the evanescent tails of bulk states outside the crystal or the presence of the crystal-induced surface state itself are of crucial importance. In the case of excited holes at the $n = 0$ surface-state band-edge ($\boldsymbol{k}_{\parallel} = 0$) on Cu(111) and Ag(111), coupling of the $n = 0$ surface state with the crystal occurring within the $n = 0$ surface-state band itself (intraband transition) is found to be $\sim 80\%$–90% of the total decay rate. Coupling of the $n = 1$ image-state electron at the $\overline{\Gamma}$ point with the unoccupied part of the $n = 0$ surface-state band on the (111) surfaces of Cu and Ag approximately represents 35%–40% of the total decay rate.

For comparison, we have reported decay rates of electrons or holes in three-dimensional (3D) and two-dimensional (2D) uniform systems. Our 2D calculations for the intraband decay rate of the $n = 0$ surface-state hole on Cu(111) and Ag(111) indicate that 2D decay rates are larger than the actual intraband contribution to the decay rate by a factor of ~ 7, thereby showing the key role that the screening by the underlying 3D bulk electron system plays in the decay mechanism. Our results also indicate that there is a large departure of the actual inelastic broadening of the $n = 1$ image state on Cu(111) and Ag(111) from the broadening of a bulk state of the same energy times the penetration of the image-state wave function into the bulk. This is found to be due to the existing large restriction on these surfaces that only final states with energy lying below the projected band gap are allowed.

A careful comparison between STM measurements of the $n = 0$ surface-state linewidth on the (111) surfaces of Cu and Ag with calculated results has recently been shown to yield a nice agreement, after inclusion of both electron-phonon scattering and the screening from *d*-electrons [25]. The experimental measurement for the $n = 1$ image-state lifetime on Cu(111) is found to be in excellent agreement with our prediction; however, our calculations yield a linewidth for Ag(111) that is too high. Our calculated linewidth for the $n = 1$ image state on the (0001) surface of ruthenium, which is located close to the band-gap center, is found to be in fair agreement with experiment.

Acknowledgements. We gratefully acknowledge discussions with R. Berndt. This work was partially supported by the University of the Basque Country, the Basque Hezkuntza, Unibertsitate eta Ikerketa Saila, and the Spanish Ministerio de Educación y Cultura. P.M.E. gratefully acknowledges support from the Max Planck Research Award funds.

References

1. L. Hedin, S. Lundqvist: Solid State Phys. **23**, 1 (1969)
2. H. Petek, S. Ogawa: Prog. Surf. Sci. **56**, 239 (1998)
3. P.M. Echenique, J.M. Pitarke, E.V. Chulkov, A. Rubio: Chem. Phys. **201**, 1 (2000)
4. P.M. Echenique, J.B. Pendry: J. Phys. C **11**, 2065 (1978); Prog. Surf. Sci. **32**, 111 (1990)
5. N.V. Smith: Rep. Progr. Phys. **51**, 1227 (1988)
6. V. Dose, W. Altmann, A. Goldmann, U. Kolac, J. Rogozik: Phys. Rev. Lett. **52**, 1919 (1984)
7. D. Straub, F.J. Himpsel: Phys. Rev. Lett. **52**, 1922 (1984)
8. B. Reihl, K.H. Frank, R.R. Schlitter: Phys. Rev. B **30**, 7328 (1987)
9. K. Giesen, F. Hage, F.J. Himpsel, H.J. Riess, W. Steinmann: Phys. Rev. Lett. **55**, 300 (1985); Phys. Rev. B **33**, 5241 (1986); Phys. Rev. B **35**, 971 (1987)
10. See, e.g., T. Fauster, W. Steinmann: *Electromagnetic Waves: Recent Development in Research*, Vol. 2, ed. by P. Halevi (Elsevier, Amsterdam 1995) p. 350
11. T. Hertel, E. Knoesel, M. Wolf, G. Ertl: Phys. Rev. Lett. **76**, 535 (1996)
12. M. Wolf, E. Knoesel, T. Hertel: Phys. Rev. B **54**, 5295 (1996); M. Wolf: Surf. Sci. **377**–**379**, 343 (1997)
13. E. Knoesel, A. Hotzel, M. Wolf: J. Electron. Spectrosc. Relat. Phenom. **88**–**91**, 577 (1998)
14. J.D. McNeil, R.L. Lingle, Jr., N.H. Ge, C.M. Wong, R.E. Jordan, C.B. Harris: Phys. Rev. Lett. **79**, 4645 (1997)
15. W. Berthold, U. Höfer, P. Feulner, D. Menzel: Chem. Phys. **251**, 123 (2000)
16. U. Höfer, I.L. Shumay, C. Reuss, U. Thomann, W. Wallauer, T. Fauster: Science **277**, 1480 (1997)
17. I.L. Shumay, U. Höfer, C. Reuss, U. Thomann, W. Wallauer, T. Fauster: Phys. Rev. B **58**, 13974 (1998)
18. S.D. Kevan: Phys. Rev. Lett. **50**, 526 (1983); J. Tersoff, S.D. Kevan: Phys. Rev. B **28**, 4267 (1983)

19. B.A. McDougall, T. Balasubramanian, E. Jensen: Phys. Rev. B **51**, 13 891 (1995)
20. F. Theilmann, R. Matzdorf, G. Meister, A. Goldmann: Phys. Rev. B **56**, 3632 (1997)
21. R. Matzdorf: Surf. Sci. Rep. **30**, 153 (1998)
22. A. Goldmann, R. Matzdorf, F. Theilmann: Surf. Sci. **414**, L932 (1998)
23. T. Balasubramanian, E. Jensen, X.L. Wu, S.L. Hulbert: Phys. Rev. B **57**, R6866 (1998)
24. J. Li, W.-D. Schneider, R. Berndt, O.R. Bryant, S. Crampin: Phys. Rev. Lett. **81**, 4464 (1998)
25. J. Kliewer, R. Berndt, E.V. Chulkov, V.M. Silkin, P.M. Echenique, S. Crampin: Science **288**, 1399 (2000)
26. L. Bürgi, O. Jeandupeux, H. Brune, K. Kern: Phys. Rev. Lett. **82**, 4516 (1999)
27. E.V. Chulkov, I. Sarria, V.M. Silkin, J.M. Pitarke, P.M. Echenique: Phys. Rev. Lett. **80**, 4947 (1998); I. Sarria, J. Osma, E.V. Chulkov, J.M. Pitarke, P.M. Echenique: Phys. Rev. B **60**, 11 795 (1999)
28. J. Osma, I. Sarria, E.V. Chulkov, J.M. Pitarke, P.M. Echenique: Phys. Rev. B **60**, 1059 (1999)
29. E.V. Chulkov, J. Osma, I. Sarria, V.M. Silkin, J.M. Pitarke: Surf. Sci. **433**, 882 (1999)
30. E.V. Chulkov, V.M. Silkin, P.M. Echenique: Surf. Sci. **454**–**456**, 458 (2000)
31. J. Lindhard: K. Dan. Vidensk. Selsk. Mat.- Fys. Medd. **28**, 8 (1954)
32. F. Stern: Phys. Rev. Lett. **18**, 546 (1967)
33. Equation (6) is equivalent to the corrected equation (6.15) in R.H. Ritchie: Phys. Rev. **114**, 644 (1959) (the $1/2$ factor in front of z^2 in the expansion of f_1 just before equation (6.15) of this reference must be replaced by $1/3$, as done in R.H. Ritchie, J.C. Ashley: J. Phys. Chem. Solids **26**, 1689 (1963)). Had we used for the real part of $\epsilon(\boldsymbol{q}, \omega)$ the Thomas–Fermi dielectric function, the 3D decay rate would have been given by -2 times the rhs of equation (7) in J.J. Quinn: Phys. Rev. **126**, 1453 (1962). In the high-density limit ($r_s \to 0$), (6) yields $\tau_{3D} = (263\,\mathrm{fs,\,eV^2})\, r_s^{-5/2}\,(E - E_F)^{-2}$, as calculated in J.J. Quinn, R.A. Ferrell: Phys. Rev. **112**, 812 (1958)
34. A.V. Chaplik: Zh. Eksp. Teor. Fiz. **60**, 1845 (1971) [Sov. Phys. JETP **33**, 997 (1971)]
35. G.F. Giuliani, J.J. Quinn: Phys. Rev. B **26**, 4421 (1982)
36. E.V. Chulkov, V.M. Silkin, P.M. Echenique: Surf. Sci. **391**, L1217 (1997); **437**, 330 (1999)
37. D. Pines: *Elementary Excitations in Solids* (Addison Wesley, New York 1963)
38. A.G. Eguiluz: Phys. Rev. Lett. **51**, 1907 (1983)
39. A. Goldmann, V. Dose, G. Borstel: Phys. Rev. B **32**, 1971 (1985)
40. S.L. Hulbert, P.D. Johnson, N.G. Stoffel, W.A. Royer, N.V. Smith: Phys. Rev. B **31**, 6815 (1985)
41. P.M. Echenique, J. Osma, M. Machado, V.M. Silkin, E.V. Chulkov, J.M. Pitarke: Prog. Surf. Sci. (in press)
42. The 3D decay rates of (6) coincide, for the $n = 0$ surface-state energies under study, with the full 3D RPA calculation exhibited in Table 1. The high-density limit ($r_s \to 0$) of Quinn and Ferrell (see [33]) yields linewidths of bulk excited holes at the energy of the $n = 0$ surface-state band-edge at the (111) surface of Cu and Ag of 5.8 and 0.18 meV, respectively. At the energy of the $n = 1$ image state on Cu(111) and Ag(111), the formula of Quinn and Ferrell yields linewidths of 491 and 571 meV, respectively.
43. Small differences between our full 2D RPA calculations, exhibited in Table 1, and those predicted from (8) (112 and 21 meV for Cu(111) and Ag(111), respectively), are due to the fact that for electrons at the bottom of the 2D band ($E - E_F^{3D} = -E_F^{2D}$) the condition $|E - E_F^{2D}| \ll \sqrt{E_F^{2D} \cdot q_{2D}^{TF}}$ is not fulfilled.
44. The 3D Fermi energy is (in Hartrees) $E_F \sim 1.84/r_s^2$, r_s being the so-called electron-density parameter defined by the relation $1/n_0 = (4/3)\pi(r_s a_0)^3$, n_0 being the average electron density, and a_0, the Bohr radius. For Cu and Ag, one finds $r_s = 2.67$ and 3.02, respectively.
45. I. Campillo, J.M. Pitarke, A. Rubio, E. Zarate, P.M. Echenique: Phys. Rev. Lett. **83**, 2230 (1999)